ANNALS OF GEOPHYSICS, 68, 4, DM452, 2025; doi:10.4401/ag-9307
OPEN ACCESS

Backpropagation neural network approaches for assessing petrophysical properties of a carbonate reservoir in southeast Brazil

Abel Carrasquilla[1,3], Herson Rocha[*,2]

(1) Petroleum Exploration and Engineering Laboratory (LENEP), North Fluminense State University (UENF), Rio de Janeiro, Brazil
(2) Polytechnic Institute (IPOLI), Federal University of Rio de Janeiro (UFRJ), Rio de Janeiro, Brazil
(3) National Institute of Petroleum Geophysics Science and Technology (INCT – Petroleum Geophysics), Salvador, Brazil

Article history: received February 26, 2025; accepted August 18, 2025

Abstract

This article applies backpropagation neural network algorithms to estimate petrophysical parameters, including lithology, porosity, permeability, and water saturation, in southeast Brazil's post-salt Albian carbonate reservoir. Geophysical well logs (gamma ray, bulk density, neutron porosity, deep resistivity, and sonic), petrophysical laboratory data (porosity and permeability), and geological information comprised the experimental datasets, while the water saturation was calculated with Archie's equation. Firstly, rapid interpretation of field and laboratory data provided preliminary reservoir characterization, including boundaries and average porosity. Three backpropagation neural network algorithms were then implemented to assess the petrophysical parameters. During training, validation, and testing on reference hole LI10, Levenberg-Marquardt, Scaled Conjugate Gradient, and Bayesian Regularization techniques were used to fit the petrophysical parameters using the logs as input. Results demonstrate accurate and efficient processes, with high Pearson's correlation coefficients and variable mean square error values across all parameters. Estimation of lithology, water saturation, and porosity achieved high accuracy with all algorithms, while permeability posed the greatest challenge. Bayesian Regularization yielded the best performance, followed by Levenberg-Marquardt and Scaled Conjugate Gradient, though all produced reasonable estimates. Successful blind test at well LI03 confirms these techniques as promising approaches for petrophysical characterization.

Keywords: Neural Network; Permoporous Properties; Water Saturation; Carbonate Reservoir; Campos Basin

1. Introduction

Petrophysics is not limited to the analysis of logs, but it comprehends an evaluation process within a geological context or framework, supported by adequate calibration data, including sedimentology, core analysis, and dynamic data from pressure measurements and borehole tests (Cannon, 2016). Logs do not measure lithology, porosity (ϕ), permeability (k), or water saturation (S_w) directly. Still, they make measurements of acoustic velocity, electrical conductivity, and various nuclear relationships between the rock and the fluids to allow for the process and interpret the results indirectly. The petrophysicist's role is to validate and organize the input data and to understand and calibrate the results (Yang and Wei, 2017).

Usually, diverse records respond slightly differently to other petrophysical parameters to unveil the mixture, so that the logs must be analyzed together, representing an advantage and not a weakness in the characterization of a reservoir (Tiab and Donaldson, 2004).

Over the years, many authors have discussed the benefits and difficulties of using artificial neural network (ANN) techniques combined with logs to estimate petrophysical parameters (e.g. Dell'Aversana, 2019). Among many of them, other works deserve mention, such as those of Bruce et al. (2000), which applied two models, backpropagation and radial basis function networks, to estimate k.

Rezaee et al. (2006) used a fully connected multi-layer perceptron network to predict k from ϕ and pore throat radii. Hamada and Elshafei (2009) presented a successful application of ANN to infer ϕ and k of gas sand reservoirs using nuclear magnetic resonance (NMR) and conventional open hole logs data. Yeganeh et al. (2012) used an ANN and log data as the input data, and the horizontal k obtained by coring was the target data. Mohebbi et al. (2012) got results from log data using ANN and compared them with the measured permeability in core analysis experiments.

ANN is a group of connected input/output units with weighted connections that enable the processing and learning of complex patterns (Ahmadi et al., 2012). The architecture of ANN is designed to mimic aspects of the human nervous system, allowing for robust applications in image interpretation, pattern recognition, and speech processing (Mohaghegh et al., 1994). Among the approaches to ANN, one that stands out is the Backpropagation Neural Network (BPNN), which is the essence of ANN training. In other words, BPNN in ANN is a short form for "backward propagation of errors" and is a standard method of training ANN. It is the method of fine-tuning the weights of an ANN based on the error rate obtained in the previous epoch, i.e., iteration (Silva et al., 2015).

Proper tuning of network weights is essential for minimizing error rates and enhancing model reliability through improved generalization capabilities. This process involves calculating the gradient of a loss function related to all network weights, thereby enabling elective optimization (Silva et al., 2020). The primary advantages of BPNN include its simplicity, ease of implementation, and minimal parameter tuning requirements beyond the number of inputs. Additionally, BPNN is a flexible approach that does not demand prior knowledge of the network structure, is generally robust and reliable, and does not require explicit specification of the features to be learned (Rene et al., 2013; Tweedale and Jain, 2014).

The main goal of this study is to use backpropagation neural network (BPNN) approaches to predict the petrophysical characteristics of a carbonate reservoir in Brazil's Campos Basin. This study was built upon the study of Carrasquilla and Lima (2020) by incorporating advanced BPNN algorithms for the estimation of petrophysical properties in the same Campos Basin offshore carbonate reservoir. While Carrasquilla and Lima (2020) utilized basic and specialized geophysical well logs, our approach innovatively integrates a comprehensive dataset that includes not only geophysical logs but also detailed laboratory measurements and geological data to enhance the accuracy of lithology, porosity, permeability, and water saturation assessments.

Furthermore, we employed three distinct training techniques in our neural network modeling – Levenberg-Marquardt, Scaled Conjugate Gradient, and Bayesian Regularization – allowing for a more robust validation of results. This methodological advancement demonstrates significant improvements in parameter estimation reliability and showcases the potential for applying machine learning techniques to petrophysical characterization, highlighting a new direction in reservoir assessment compared to the previous research.

2. Geological and petrophysical characterization

This study was developed in the Campos Basin, which produces 40% of Brazil's oil. The basin is along the continental margin in Southeastern Brazil, and a dashed red rectangle marks the position of Linguado Oilfield in Fig. 1. Its Albian carbonate reservoirs of the Quissama Formation are productive within the basin, with an average porosity and permeability of 25% and 25 mD, respectively (Bruhn et al., 2003).

The sedimentation of this carbonate started in the drift phase at the beginning of Albian with marine deposition (Fig. 2a). The depositional environment is a carbonate ramp originated by sedimentary processes occurring under high, medium, and low energy (Fig. 2b). The lithology correspondences are, respectively, oolitic and oncolytic grainstones, oolitic peloidal grainstones and oncolytic bioclastic packstones, and peloidal bioclastic packstones and wackestones (Okubo et al., 2015).

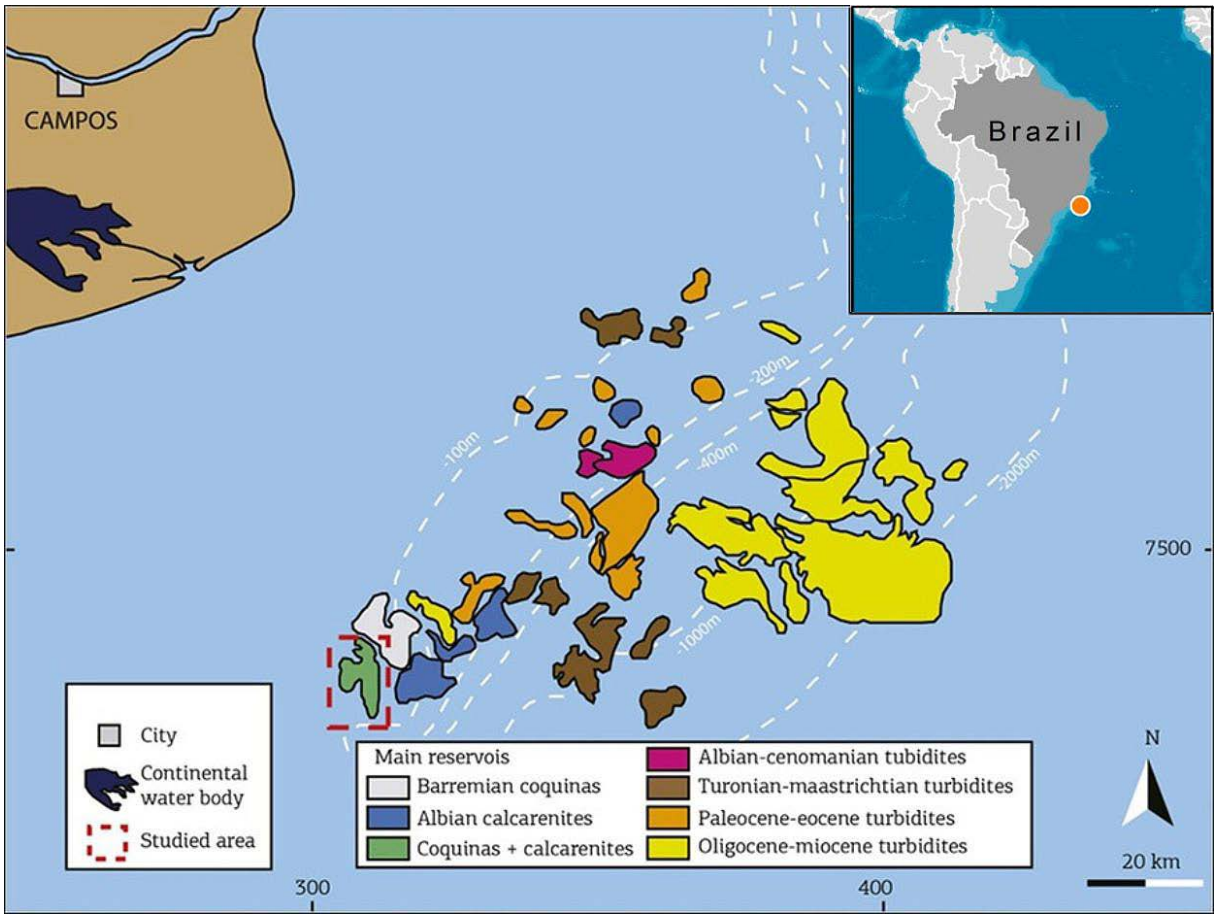

Figure 1. Location map of the area studied in the southwestern portion of Campos Basin, with the Linguado oilfield highlighted in the dashed red rectangle (modified from Bruhn et al., 2003; Carrasquilla and Lima, 2020).

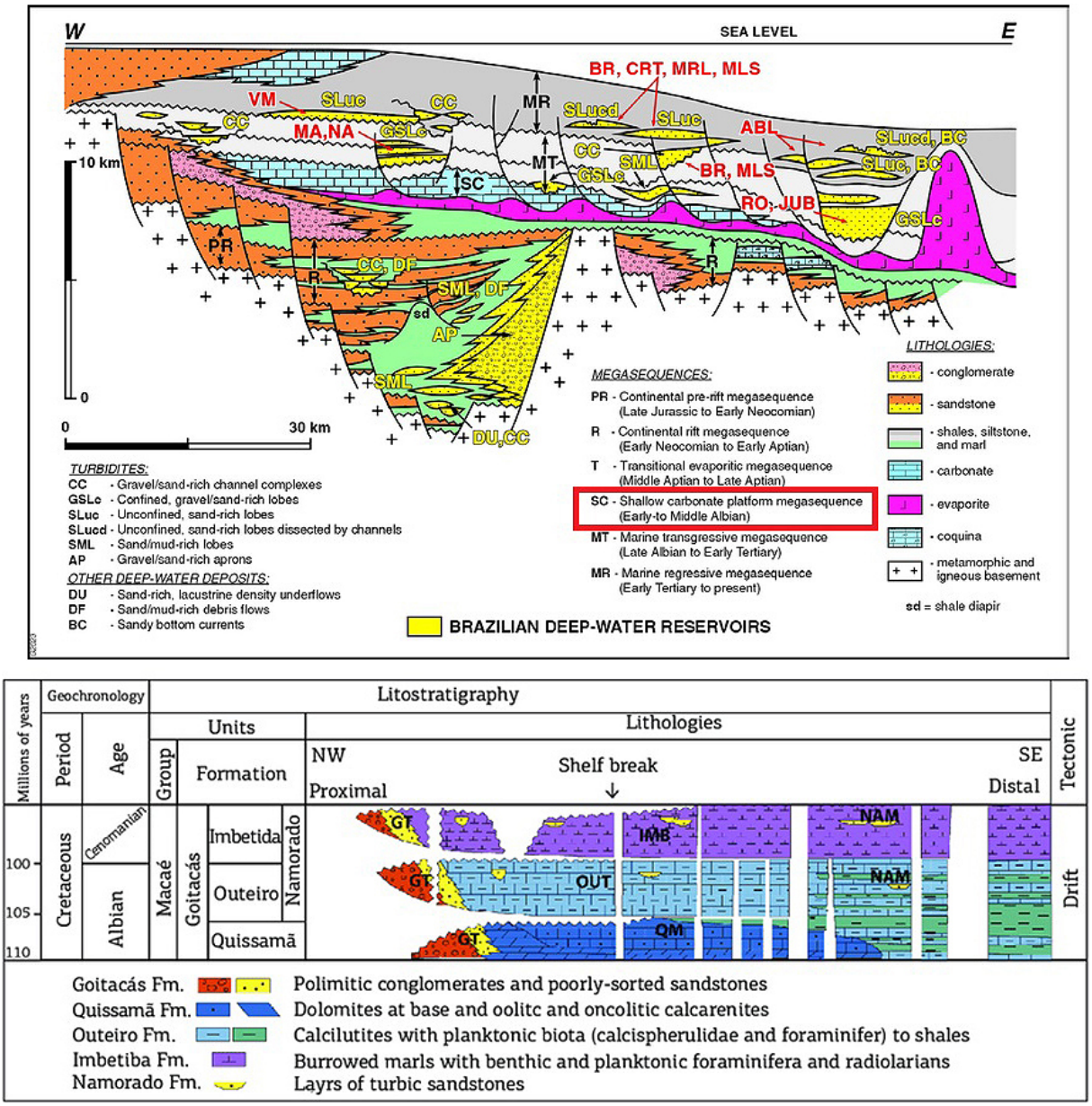

Figure 2. Typical geological section of Southeast Brazil (above) and part of the Campos Basin stratigraphic chart (below), highlighting the red rectangle that contains the shallow carbonates platform (modified from Bruhn et al., 2003; Winter et. al., 2007; Okubo et al., 2015; Carrasquilla and Lima, 2020).

3. Materials and Methods

The dataset to study this reservoir consists of logs, laboratory data, and geological information from wells LI10 and LI03. The first is considered a reference well, and the other is the blind test well (ANP, 2019). The reference borehole is focused within the carbonate island because it has a complete suite of basic logs and petrophysical measurements made in the laboratory.

Figure 3 shows the workflow of this article. On the left side, we have the input with all the logs, the laboratory measurements, and the complementary geological information (lithofacies, etc.). Next, the logs were processed using data mining principles, such as filtering and smoothing to eliminate spurious values, using wavelet transforms and cubic interpolation (Howard and Beale, 2000).

The dataset was then first interpreted and examined from a petrophysical perspective; that is, quantitatively examining these parameters allows for the establishment of relationships between them. After that, on the right side of this figure, the modeling process of the petrophysical parameters of a carbonate reservoir is shown with the BPNN approaches of Levenberg-Marquardt, Scaled Conjugate Gradient, and Bayesian Regularization (Luthi and Bryant, 1997; Beale et al., 2017). We used TrainLM, TrainSCG, and TrainBR Matlab functions are the respective training functions of Matlab software (2014).

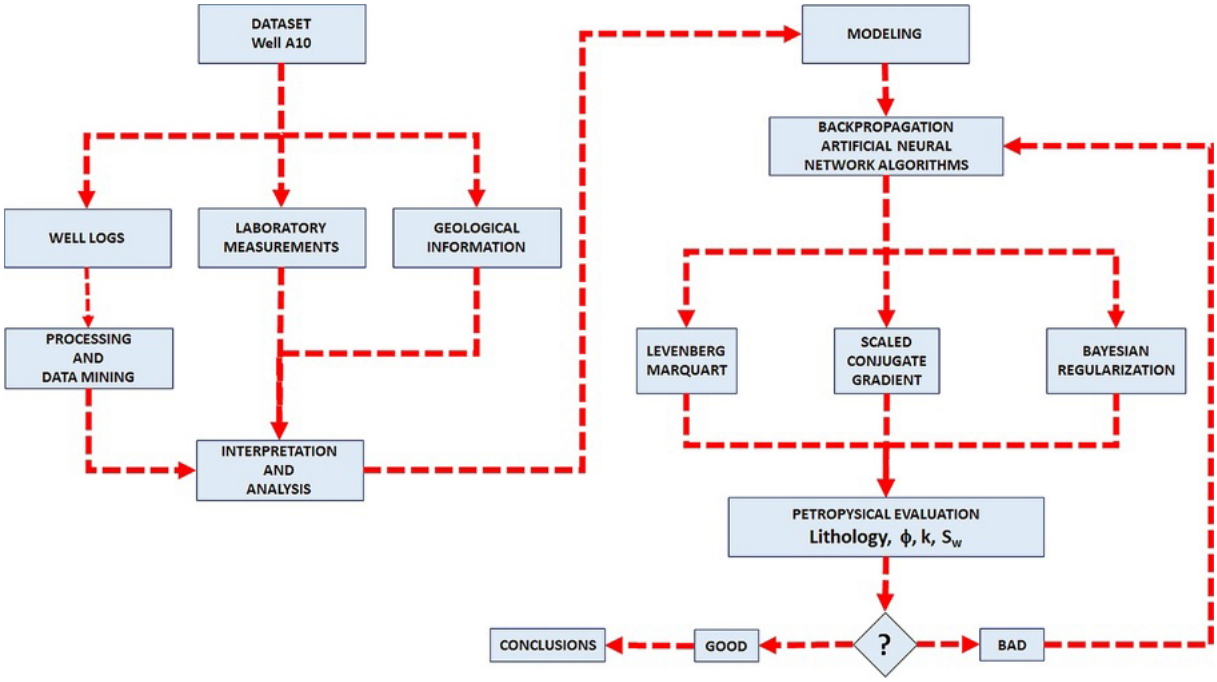

Figure 3. Workflow adopted for the present work.

The input data were logs, and the output data were petrophysical parameters measured in the laboratory (Figs. 4a and 4b). Pearson's correlation coefficient (R) and mean square error (MSE) were used to assess the quality of the estimations, or the petrophysical evaluation (Martinez and Martinez, 2001). The workflow ends if these two parameters yield encouraging findings; if not, the cycle restarts from the beginning of the modeling process (Draper, 1998).

The trainLM is an iterative technique to find the minimum of a multivariate error function E, which is the sum of the squares of the difference between the actual output (y) and the target output (t):

$$E = \frac{1}{2}\sum_{i=1}^{n}(y_i - t_i)^2 \tag{1}$$

where n is the number of parameters.

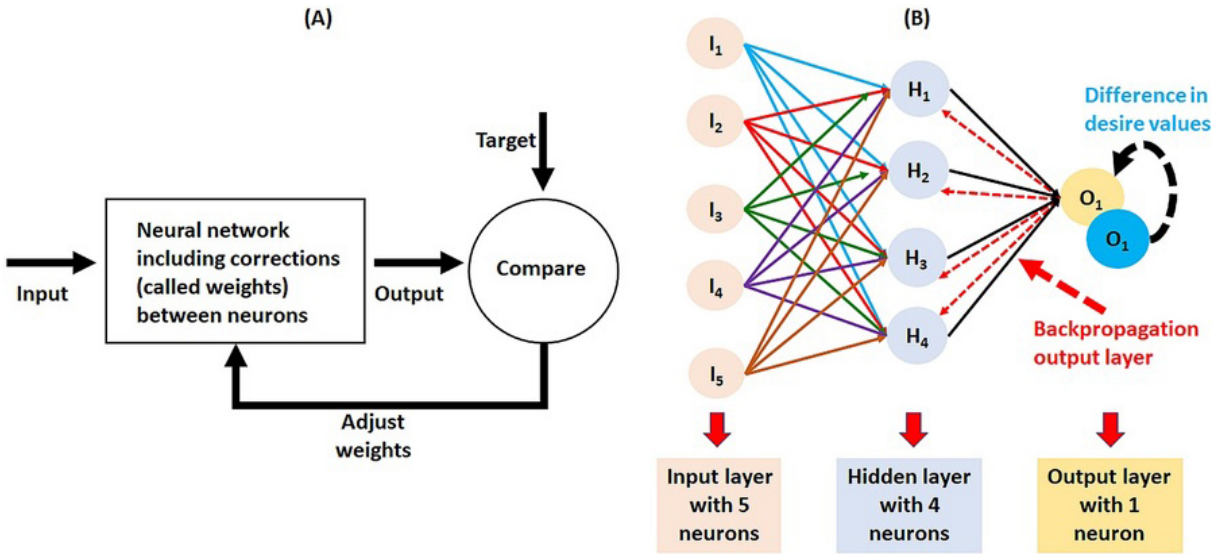

Figure 4. General scheme of artificial neural networks (A) and schematic representation of the back-propagation artificial neural network model (B).

The trainLM approximates second-order velocity without the need to compute the Hessian matrix (H). However, both H and the gradient (g) can be reached using Eqs. (2) and (3), respectively, when the performance function has a sum-of-squares form, in the following way:

$$H = J^T J \tag{2}$$

$$g = \nabla E = J^T e \tag{3}$$

where J is the Jacobian matrix containing the first derivatives of the errors concerning biases and weights, and e is the network error vector (Peng et al., 2008). Calculating J than H using a standard backpropagation method is much simpler. The trainLM algorithm uses this approximation for H in the following Newton-type update:

$$w_{i+1} = w_i - [J^T J + \mu I]^{-1} J^T e \tag{4}$$

where w represents the connection weights, μ is the damping term, and I is the identity matrix.

The trainLM uses the Gauss-Newton method and gradient descent in its iterative process. When μ is zero, it becomes a Gauss-Newton method using the approximate H. When the parameter μ is large, the algorithm operates as a gradient descent method with a reduced step size. In contrast, Newton's method demonstrates superior convergence speed and precision, achieving near-minimal error.

$$\bar{s}_k = \frac{E'(\bar{w}_k + \sigma_k \bar{p}_k) - E'(\bar{w}_k)}{\sigma_k} + \lambda_k \bar{p}_k \tag{5}$$

where λ_k is a scalar and is adjusted each time according to the sign of λ_k, σ_k is a small scaling factor (perturbation size) for finite differences to approximate curvature, and $\bar{p}_k$ is the search direction (conjugate gradient direction) at iteration k. In this algorithm, the step size is a function of a quadratic approximation of the error function, which

makes it more robust and independent of user-defined parameters. The step size is estimated using a different approach:

$$\alpha_k = \frac{\mu_k}{\delta_k} = \frac{-\bar{p}_j^T E'_{qw}(\bar{y}_1)}{\bar{p}_j^T E'_{qw}(\bar{w}) p_j} \tag{6}$$

where $\bar{w}$ is weight vector in space R^n, the $E(\bar{w})$ is the global error function, the $E'(\bar{w})$ is the gradient of error, the $E'_{qw}(\bar{y}_1)$ is the quadratic approximation of the error function, the $\bar{p}_1, \bar{p}_2, \ldots, \bar{p}_k$ are the set of non-zero weight vectors. The λ_k is to be updated such that,

$$\bar{\lambda}_k = 2\left(\lambda_k - \frac{\delta_k}{|p_k|^2}\right) \tag{7}$$

If $\Delta_k > 0.75$, then $\lambda_k = \frac{\lambda_k}{4}$. If $\Delta_k < 0.25$, then $\lambda_k = \lambda_k + \left(\frac{\delta_k(1-\Delta_k)}{|p_k|^2}\right)$, where Δ_k is comparison parameter and is given by Eq. (8):

$$\Delta_k = \frac{2\delta_k[E(\bar{w}_k) - E(\bar{w}_k + \sigma_k \bar{p}_k)]}{\mu_k^2} \tag{8}$$

Initially, the parameters are set as $0 < \sigma \leq 10^{-4}$, $0 < \lambda_l \leq 10^{-6}$, and $\lambda_l = 0$. The training process terminates when any of the following conditions are met: (i) the maximum number of epochs is reached, (ii) the maximum allowable time is exceeded, (iii) the performance function achieves the predefined goal, (iv) the gradient of the performance function falls below the specified minimum threshold (min-grad), and (v) the validation performance has increased more than the maximum allowable failures (max-fail) since the last time it decreased, provided validation is being used (Babani et al., 2016).

The trainBR algorithm is a training method that adjusts weights and bias values using the trainLM optimization technique. It minimizes a combination of squared errors and weight magnitudes, determining the optimal balance to ensure robust network generalization. According to Foresee and Hagan (1997), this approach to enhancing generalization is referred to as regularization.

The primary objective of training is to minimize the sum of squared errors, denoted as E_D. In this context, the training objective function is initially expressed as $F = E_D$. However, with regularization, an additional term, E_w, is incorporated to penalize large weights. The modified objective function is then given as:

$$F = \beta E_D + \alpha E_w \tag{9}$$

where E_w is the sum of the squares of the network weights, the E_D is the sum of network errors, and α and β are the regularization parameters that balance the trade-off between minimizing errors and preventing overfitting. This regularization approach ensures improved generalization by discouraging overly complex models (Kaur and Salaria, 2013).

Foresee and Hagan (1997) explain that the relative magnitudes of the objective function parameters determine the focus of the training process. When $\alpha \ll \beta$, the training algorithm prioritizes reducing errors in the network outputs. Conversely, when $\alpha \gg \beta$, the algorithm emphasizes minimizing weight magnitudes at the expense of network accuracy, resulting in a smoother network with potentially reduced overfitting.

A key challenge in applying regularization lies in determining the appropriate values for these objective function parameters. Foresee and Hagan (1997) address this by employing Bayes' rule, which offers a systematic framework for updating probabilistic beliefs based on new relevant evidence.

This approach enables robust and adaptive optimization of the parameters α and β, ensuring an effective balance between error minimization and weight regularization during training. When prior information is available, Bayesian methods allow for its integration and refinement with additional data, leading to improved parameter estimation (Masoudi et al., 2012).

4. Results

4.1 Field logs and laboratory measurements

The logs between tracks A to E were gamma-ray (GR, in °API), density (RHOB, in g/cm^3), neutron porosity (NPHI, in %), deep resistivity (RT, in Ωm) (Da Costa et al., 2019), and sonic (DT, in msec/feet). Lithology is in track F, classified according to Okubo et al. (2015). The water saturation S_w (%) is calculated using Archie's (1942) equation using RT and RHOB logs because we do not have laboratory measurements of this parameter (track G). The laboratory data correspond to porosity ϕ_{LAB} (%) and permeability k_{LAB} (mD) in tracks H and I, respectively (ANP, 2019).

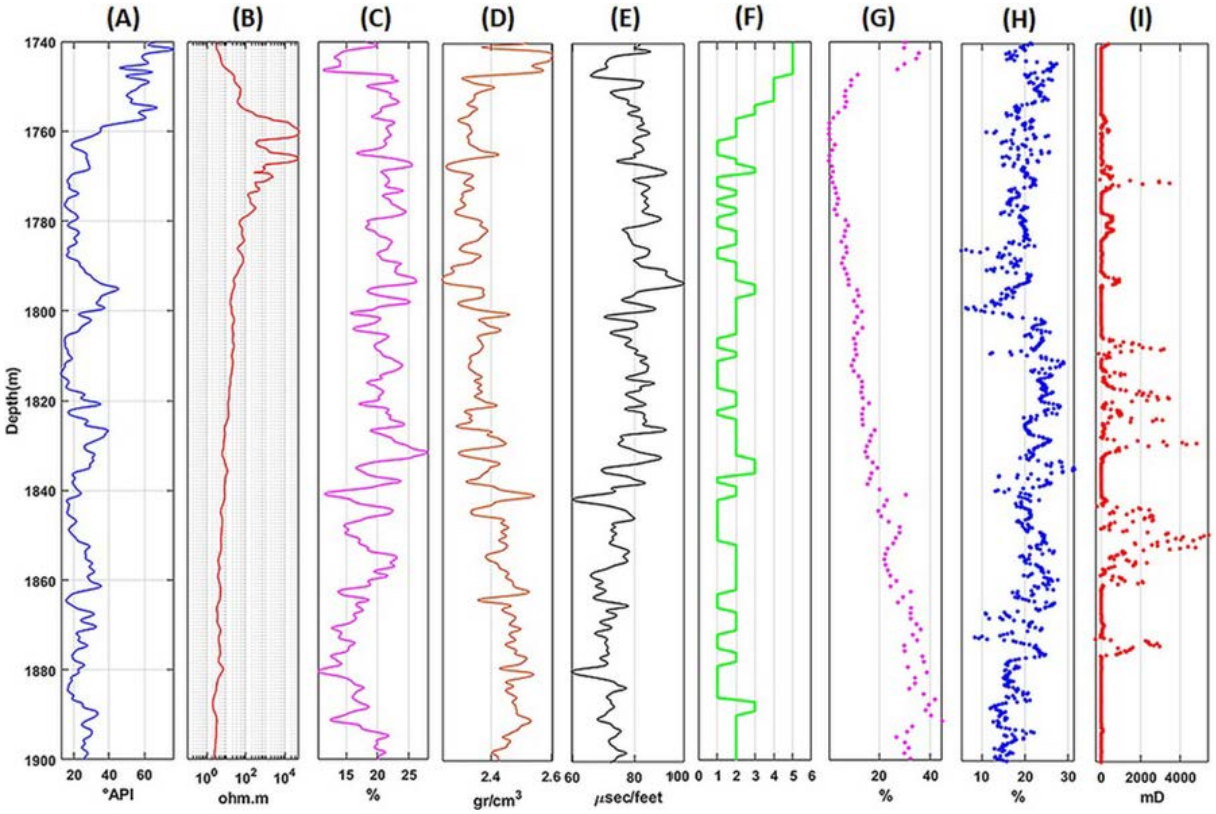

Figure 5. Data set used in this work: (a) gamma-ray, (b) resistivity, (c) neutron porosity, (d) bulk density, (e) sonic log, (f) Okubo's lithology, (g) Archie water saturation, (h) porosity, and (i) permeability measured in the laboratory.

The GR log (Fig. 5a) exhibits an abrupt decrease at approximately 1760 m depth, marking the onset of the reservoir interval. Additionally, the resistivity drastically increases between 1760 and 1780 m of depth (Fig. 5b), rising from values below 10 Ω·m to over 10^4 Ω·m, which strongly indicates the presence of hydrocarbons. Within this interval, the NPHI log (Fig. 5c) indicates an average porosity of 23% within the same depth range, while the RHOB log (Fig. 5d) presents an average value of 2.4 g/cm^3, consistent with typical limestone density values (1.93 to 2.90 g/cm^3).

The sonic DT log (Fig. 5e) varies from 60 to 100 μsec/feet, revealing a notable reduction at 1740 m depth, suggesting an increase in porosity, characteristic of reservoir rocks. Integrating the log responses, the hydrocarbon-bearing zone is identified between 1750 and 1800 m depth. The transition zone extends from 1800 to 1860 m depth, with the aquifer zone located below 1860 m depth, confirming the delineation of the reservoir and its associated fluid zones.

Figure 5f illustrates the lithology of well LI10, which is categorized as follows: grainstone (1), cemented grainstone (2), packstone (3), cemented packstone (4), and wackestone (5). The water saturation (S_w) log, shown in Fig. 5g, highlights an upper section, characterized by wackestone, where S_w is high, while water saturation decreases to values below 10% between 1760 and 1790 m depth, corresponding to the grainstone reservoir, where oil saturation is predominant. The transition zone extends from 1800 to 1850 m depth, beyond which S_w reaches 100%, indicating the aquifer zone below 1860 m depth.

The porosity measurements achieved from laboratory analysis (Fig. 5h) exhibit significant oscillations, closely reflecting the stratigraphic variations. The average porosity is approximately 20%, with some intervals showing lower values around 10% and others reaching higher values up to 30%. These variations underscore the heterogeneity of the reservoir and its associated lithologies.

Laboratory-measured permeability (Fig. 5i) is predominantly low (~0 mD) across most depths but exhibits distinct peaks at specific intervals. Permeability reaches approximately 300 mD at depths of 1770, 1810, 1820, and 1870 m, with significant peaks of up to 5000 mD observed at depths of 1830 and 1850 m. These peaks largely correspond to grainstone or cemented grainstone layers, as indicated in Fig. 5f.

4.2 Lithology estimation

Figure 6 illustrates the lithology estimation process utilizing two distinct algorithms: (a) Levenberg-Marquardt (trainLM) and (b) Bayesian Regularization (trainBR). The methodologies employed, including trainLM, Scaled Conjugate Gradient (trainSCG), and trainBR, are structured into well-defined stages that encompass data sampling for validation, training, and testing (Fig. 6a). This systematic approach ensures that the algorithms are accurately refined and evaluated throughout the modeling process, facilitating reliable lithology predictions.

In contrast, the Bayesian Regularization algorithm operates without a separate validation phase (Fig. 6b). It inherently addresses the challenge of overfitting by incorporating a regularization component within the training process itself. This characteristic allows Bayesian Regularization to effectively manage model complexity while enhancing the accuracy of lithology estimations. By integrating these robust techniques, the study aims to improve the reliability of petrophysical parameter assessments, providing valuable insights for reservoir characterization.

Figure 7 presents the lithology estimation results obtained using trainLM (a), trainSCG (b), and trainBR (c) algorithms, with detailed outcomes summarized in Table 1.

The high accuracy in lithology determination is likely attributed to the clean and well-distributed target data, derived from detailed geological observations. These results indicate strong performance across all algorithms, with trainBR demonstrating a marginally superior performance compared to trainLM and trainSCG when all metrics are considered. The findings underscore the effectiveness of the proposed methods in lithology estimation and the robustness of trainBR in particular.

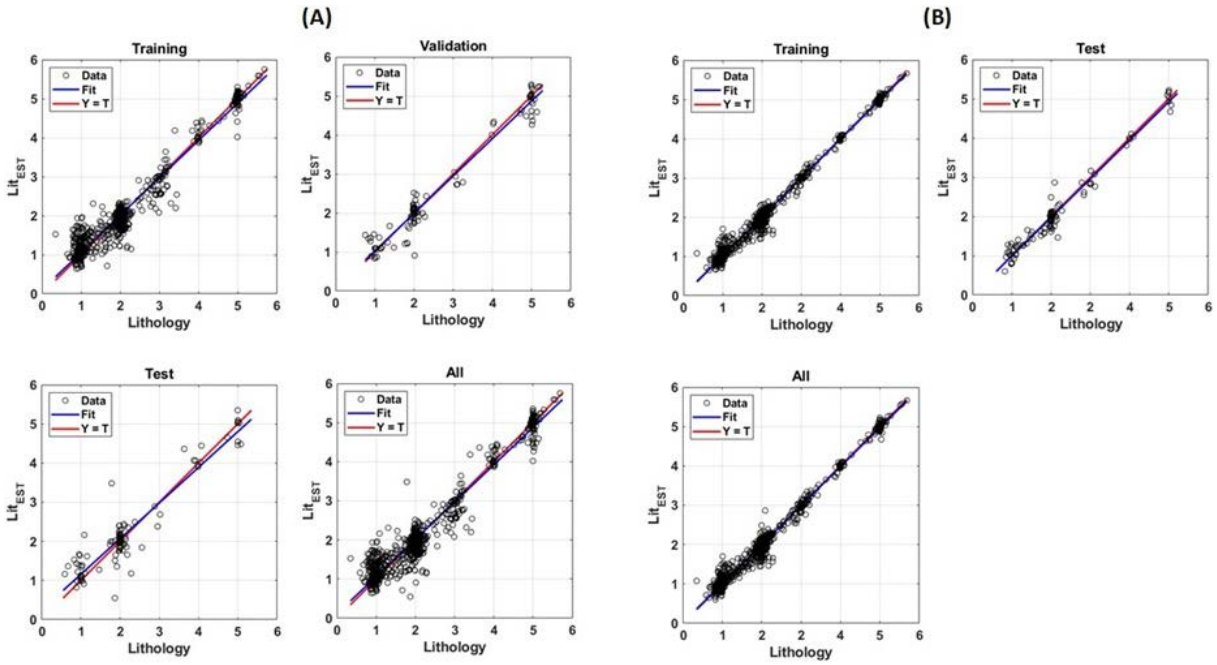

Figure 6. Lithology estimates for reference well LI10 showing (a) Levenberg-Marquardt and (b) Bayesian Regularization schemes.

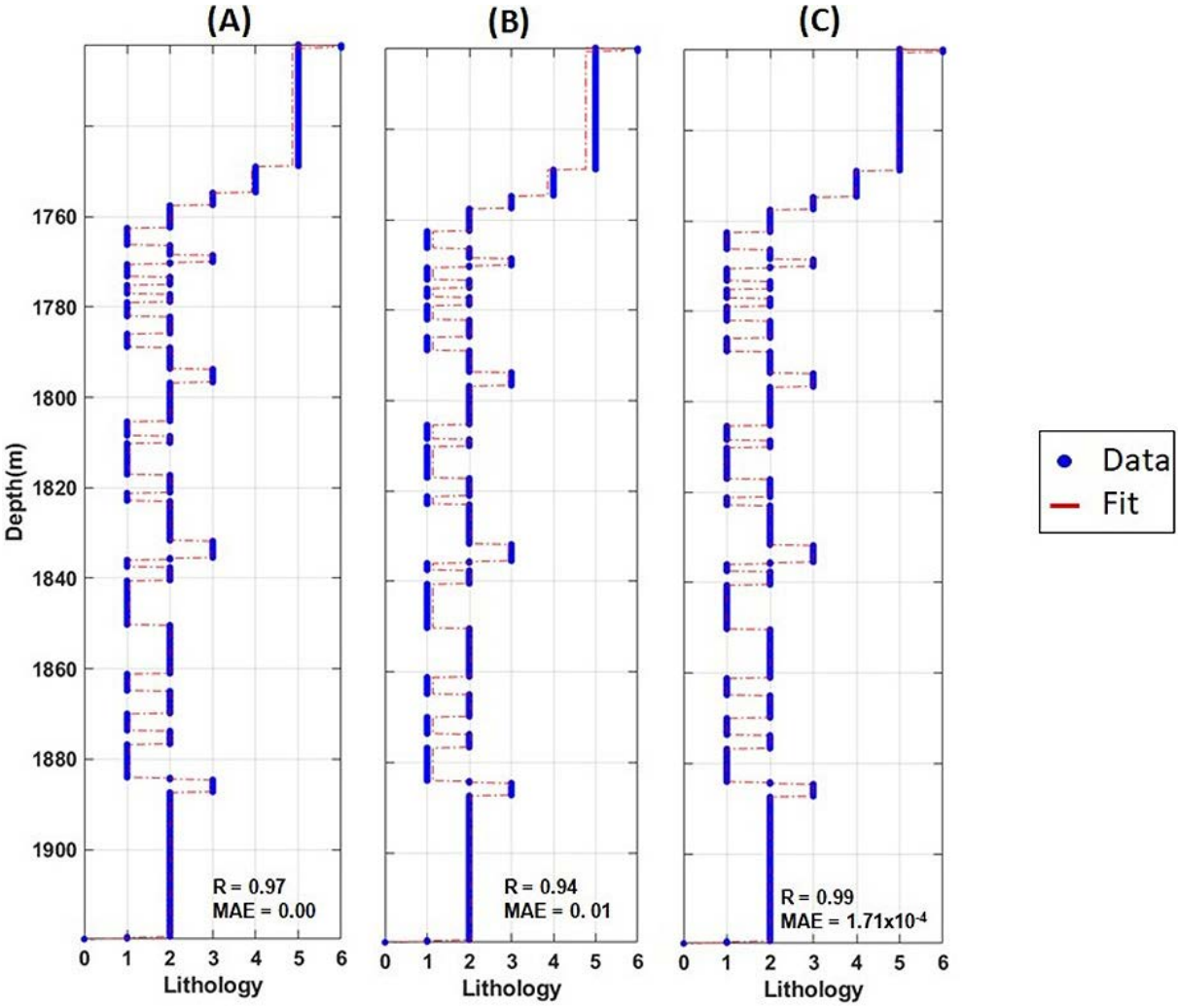

Figure 7. Lithology estimates for the reference well LI10: (a) Levenberg-Marquart, (b) Scaled Conjugate Gradient, and (c) Bayesian Regularization schemes.

Table 1. Lithology determinations with different approaches for the reference well LI10.

Levenberg-Marquardt					Scaled Conjugate Gradient				Bayesian Regularization			
Units	**Samples**	**Equations**	**R**	**MSE**	**Samples**	**Equations**	**R**	**MSE**	**Samples**	**Equations**	**R**	**MSE**
Training	792	0.96(Litho) + 0.10	0.98	0.07	792	0.91(Litho) + 0.22	0.94	0.19	891	0.99(Litho) + 0.03	1.00	0.03
Validation	99	0.96(Litho) + 0.08	0.98	0.09	99	0.89(Litho) + 0.24	0.94	0.17	—	—	—	—
Test	99	0.91(Litho) + 0.25	0.94	0.16	99	0.91(Litho) + 0.23	0.91	0.23	99	0.98(Litho) + 0.01	0.98	0.04
All	990	0.95(Litho) + 0.11	0.97		990	0.91(Litho) + 0.22	0.94		990	0.99(Litho) + 0.02	0.99	
Epoch	29 of 1000				90 of 1000				1000 of 1000			
Elapsed time	00:00:01				00:00:01				00:01:05			
Layer size	100				100				100			
Performance	761 to 0.02				560 to 0.19				113 to 0.0156			
Gradient	1.22×10^3 to 0.18				1.02×10^3 to 0.66				406 to 0.0157			
μ	0.001 to 0.0001								0.001 to 0.0001			
Validation checks	6				6							
Effective # param									701 to 278			
Sum squared param									1.69×10^3 to 1.40×10^3			

4.3 Porosity estimation

We report in Fig. 8 the results of the porosity (ϕ) estimation, with detailed outcomes provided in Table 2. Estimating ϕ proved to be more challenging than lithology, likely due to a broader data distribution or the inherently approximate and smoothed nature of the lithology model. Despite these difficulties, the results highlight the effectiveness of trainBR in achieving superior accuracy, further demonstrating its robustness in handling more complex parameter estimations.

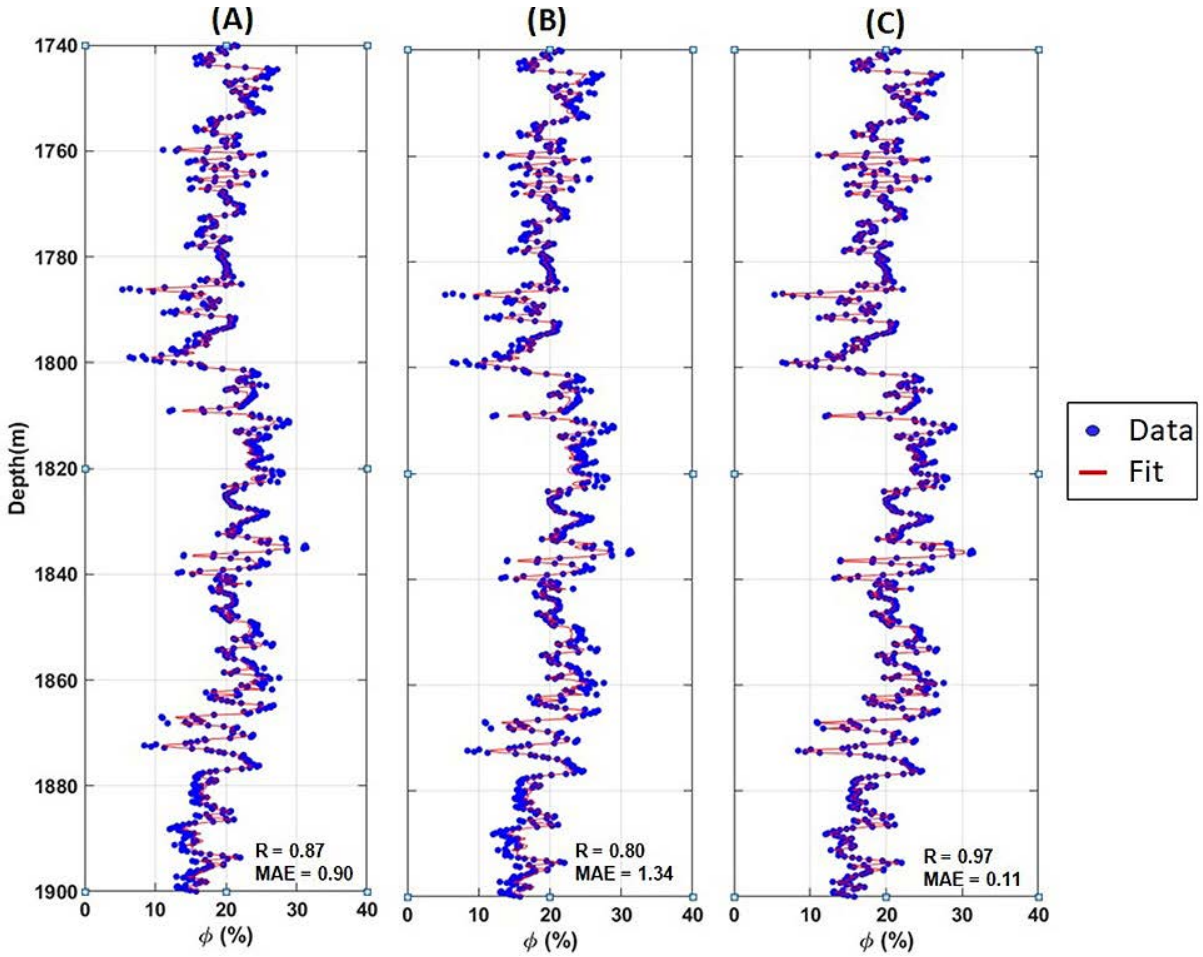

Figure 8. Porosity estimates for the reference well LI10: (a) Levenberg-Marquart, (b) Scaled Conjugate Gradient, and (c) Bayesian Regularization schemes.

Table 2. Porosity determinations with different approaches for the reference well LI10.

Levenberg-Marquardt					Scaled Conjugate Gradient				Bayesian Regularization			
Units	**Samples**	**Equations**	**R**	**MSE**	**Samples**	**Equations**	**R**	**MSE**	**Samples**	**Equations**	**R**	**MSE**
Training	792	$0.77(\phi_{LAB}) + 4.60$	0.88	3.99	712	$0.73(\phi_{LAB}) + 5.30$	0.83	6.29	891	$0.94(\phi_{LAB}) + 1.20$	0.97	1.03
Validation	99	$0.83(\phi_{LAB}) + 3.60$	0.81	6.76	139	$0.80(\phi_{LAB}) + 4.10$	0.73	8.05	—	—	—	—
Test	99	$0.80(\phi_{LAB}) + 4.00$	0.83	6.91	139	$0.67(\phi_{LAB}) + 6.20$	0.71	8.51	99	$0.91(\phi_{LAB}) + 1.50$	0.93	2.59
All	990	$0.78(\phi_{LAB}) + 4.40$	0.87		990	$0.73(\phi_{LAB}) + 5.30$	0.80		990	$0.93(\phi_{LAB}) + 1.20$	0.97	
Epoch	18 of 1000				136 of 1000				1000 of 1000			
Elapsed time	00:00:08				00:00:01				00:01:05			
Layer size	335				345				100			
Performance	9.78×10^3 to 3.22				5.52×10^3 to 6.03				2.19×10^3 to 1.03			
Gradient	3.11×10^4 to 6.24				1.34×10^4 to 20.30				4.84×10^3 to 1.83			
μ	0.001 to 0.01								0.005 to 0.5			
Validation checks	6				6							
Effective # param									701 to 340			
Sum squared param									1.69×10^3 to 2.31×10^3			

4.4 Permeability estimation

The permeability (k) estimation results are shown in Fig. 9 and summarized in Table 3. Determining k proved to be more complex than estimating lithology or ϕ, likely due to the wider spread of the target data. While the R values indicate reasonable correlations, the high MAE values across all three methods suggest that the estimates are not entirely reliable. Consequently, these results can be considered suboptimal, with trainLM showing slightly better performance compared to trainBR and trainSCG. These findings underscore the challenges associated with accurately estimating k and the limitations of the applied methods in handling this parameter.

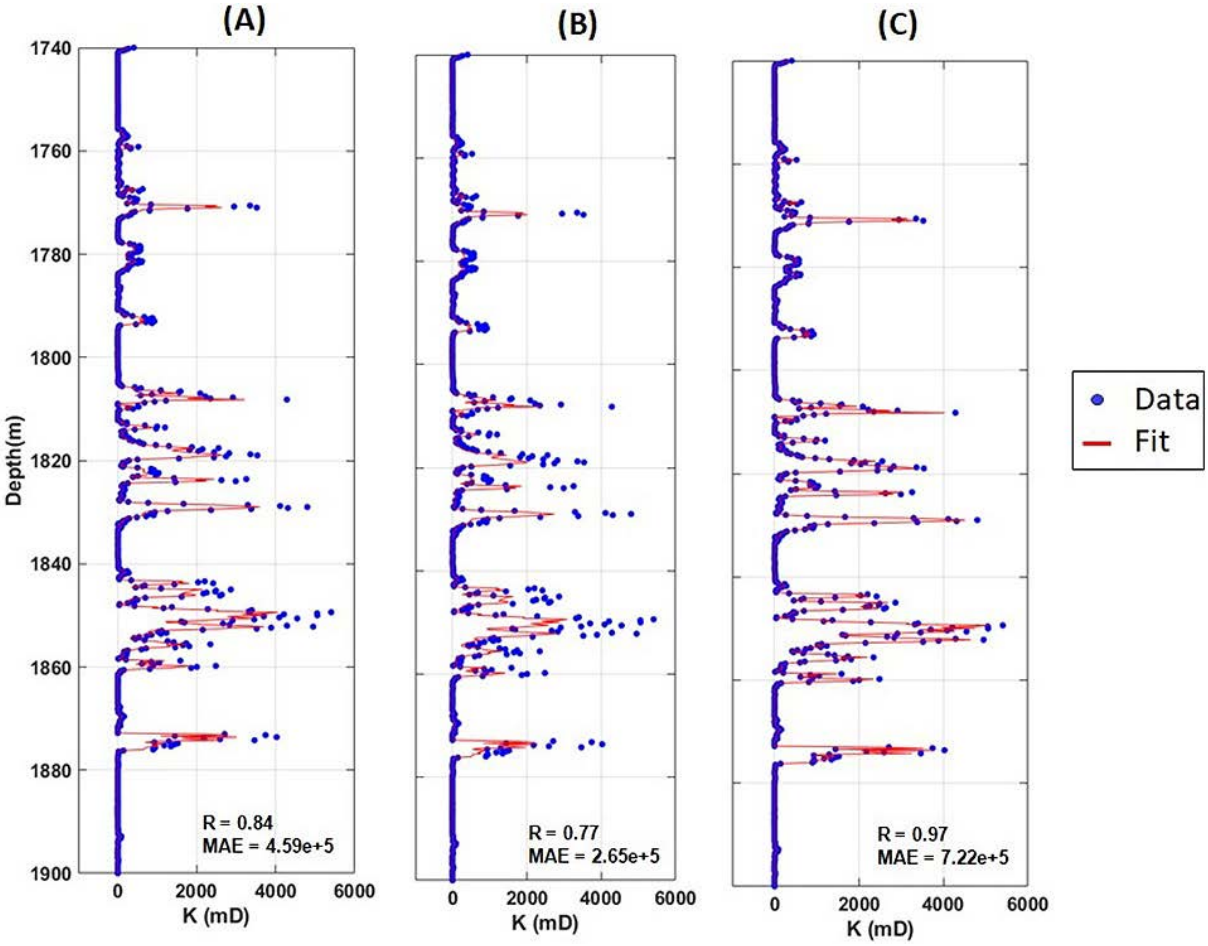

Figure 9. Permeability estimates for reference well LI10: (a) Levenberg-Marquardt, (b) Scaled Conjugate Gradient, and (c) Bayesian Regularization schemes.

Table 3. Permeability determinations with different approaches for the reference well LI10.

Levenberg-Marquardt					Scaled Conjugate Gradient				Bayesian Regularization			
Units	**Samples**	**Equations**	**R**	**MSE**	**Samples**	**Equations**	**R**	**MSE**	**Samples**	**Equations**	**R**	**MSE**
Training	792	$0.77(k_{LAB}) + 0.32$	0.88	0.41	732	$0.59(k_{LAB}) + 0.49$	0.78	0.70	891	$0.94(k_{LAB}) + 0.07$	0.97	0.09
Validation	99	$0.62(k_{LAB}) + 0.47$	0.81	0.90	129	$0.52(k_{LAB}) + 0.63$	0.75	0.83	—	—	—	—
Test	99	$0.70(k_{LAB}) + 0.29$	0.68	1.27	129	$0.57(k_{LAB}) + 0.57$	0.73	0.70	99	$0.88(k_{LAB}) + 0.12$	0.89	0.38
All	990	$0.75(k_{LAB}) + 0.33$	0.84		990	$0.57(k_{LAB}) + 0.52$	0.77		990	$0.94(k_{LAB}) + 0.07$	0.97	
Epoch	22 of 1000				97 of 1000				1000 of 1000			
Elapsed time	00:00:02				00:00:01				00:01:11			
Layer size	100				120				100			
Performance	328 to 0.312				87.7 to 0.69				50.40 to 0.09			
Gradient	713 to 1.62				378 to 0.87				242 to 0.01			
μ	0.001 to 0.0001								0.005 to 0.5			
Validation checks	6				6							
Effective # param									701 to 338			
Sum squared param									1.69×10^3 to 3.06×10^3			

4.5 Water saturation

Figure 10 displays the S_w estimation results using (a) trainLM, (b) trainSCG, and (c) trainBR algorithms, with detailed results provided in Table 4. The performance metrics for S_w estimation include correlation coefficients (R) of 0.95, 0.93, and 1.00, and mean squared error (MSE) values of 27.73, 21.06, and 4.74×10^{-9}, respectively.

Estimating S_w proved to be comparable to, if not slightly better than, lithology determination. The high R values indicate excellent correlation, and the MSE values are reasonable, reflecting reliable adjustments. Overall, these estimates are of high quality, with trainBR performing slightly better, trainLM yielding similar results, and trainSCG showing slightly lower performance. These findings affirm the robustness of the algorithms, particularly trainBR, in accurately estimating S_w.

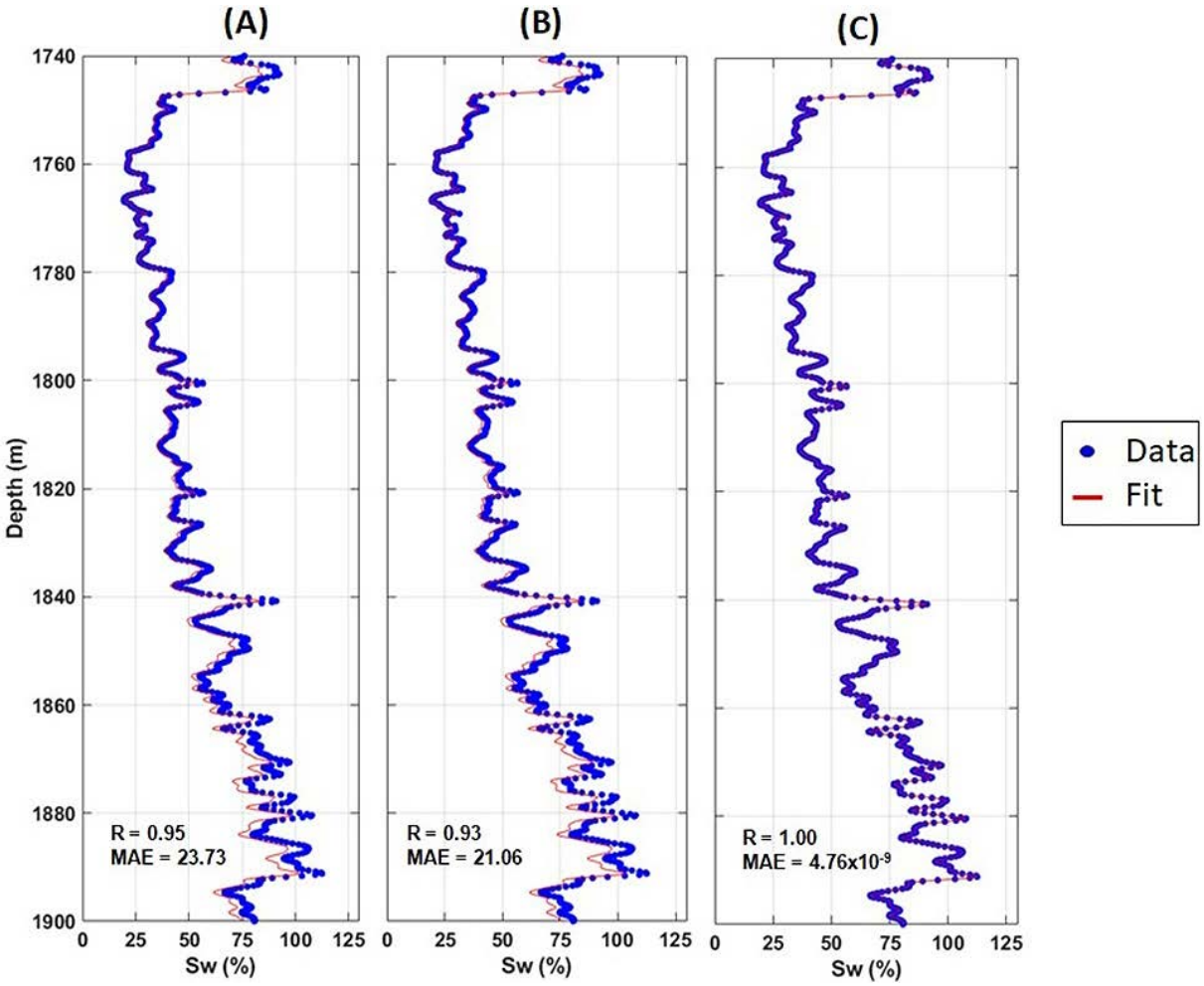

Figure 10. Water saturation estimates for the reference well LI10: (a) Levenberg-Marquardt, (b) Scaled Conjugate Gradient, and (c) Bayesian Regularization scheme.

Table 4. Water saturation determinations with different approaches for the reference well LI10.

Levenberg-Marquardt					Scaled Conjugate Gradient				Bayesian Regularization			
Units	**Samples**	**Equations**	**R**	**MSE**	**Samples**	**Equations**	**R**	**MSE**	**Samples**	**Equations**	**R**	**MSE**
Training	792	$0.88(Sw_{ARCHIE}) + 2.90$	0.88	0.00	792	$0.90(Sw_{ARCHIE}) + 2.00$	0.94	16.96	891	$(Sw_{ARCHIE}) + 1.50 \times 10^{-5}$	1.0	8.27×10^{-6}
Validation	99	$0.86(Sw_{ARCHIE}) + 3.10$	0.81	6.50	99	$0.93(Sw_{ARCHIE}) + 0.75$	0.94	17.82	—	—	—	—
Test	99	$0.91(Sw_{ARCHIE}) + 3.00$	0.83	5.13	99	$0.94(Sw_{ARCHIE}) + 1.10$	0.91	31.79	99	$(Sw_{ARCHIE}) + 3.70 \times 10^{-4}$	1.0	1.11×10^{-5}
All	990	$0.88(Sw_{ARCHIE}) + 2.90$	0.87		990	$0.90(Sw_{ARCHIE}) + 1.80$	0.94		990	$(Sw_{ARCHIE}) + 6.90 \times 10^{-5}$	1.0	
Epoch	10 of 1000				89 of 1000				1000 of 1000			
Elapsed time	00:00:01				00:00:01				00:01:07			
Layer size	100				200				100			
Performance	5.52×10^{3} to 10.80				1.04×10^{4} to 16.60				1.69×10^{4} to 8.27×10^{-6}			
Gradient	1.99×10^{4} to 17.00				3.06×10^{4} to 31.30				1.74×10^{5} to 0.02			
μ	0.001 to 0.1								0.005 to 500			
Validation checks	6				6							
Effective # param									701 to 155			
Sum squared param									1.69×10^{3} to 444			

4.6 Blind test

The results for well LI03, which functioned as a blind test, are presented in Fig. 11, showcasing estimations for four vital parameters: (a) lithology, (b) porosity, (c) permeability, and (d) water saturation. These assessments were conducted using the Bayesian Regularization approach, renowned for its effectiveness in the context of the reference well LI10, where it yielded the best performance among various methods. The application of this sophisticated technique not only provides reliable predictions but also demonstrates the method's versatility in accurately capturing the complexities of the layers' characteristics in carbonate reservoirs.

The metrics obtained from the blind test reveal a consistency in performance across all examined parameters. Specifically, the correlation coefficient (R) for each parameter equaled 1.00, reflecting a perfect alignment between the predicted values and the actual measurements. This level of correlation serves as a testament to the accuracy and reliability of the Bayesian Regularization method in petrophysical estimations.

The mean squared error (MSE) values further underscore the effectiveness of the Bayesian Regularization technique. For lithology, the MSE was recorded at 1.70×10^{-3}, while porosity exhibited an MSE of 518.56. The permeability yielded an MSE of 1.16×10^{-11}, indicating a highly accurate prediction. Additionally, the MSE for water saturation was documented at 1.69×10^{-6}.

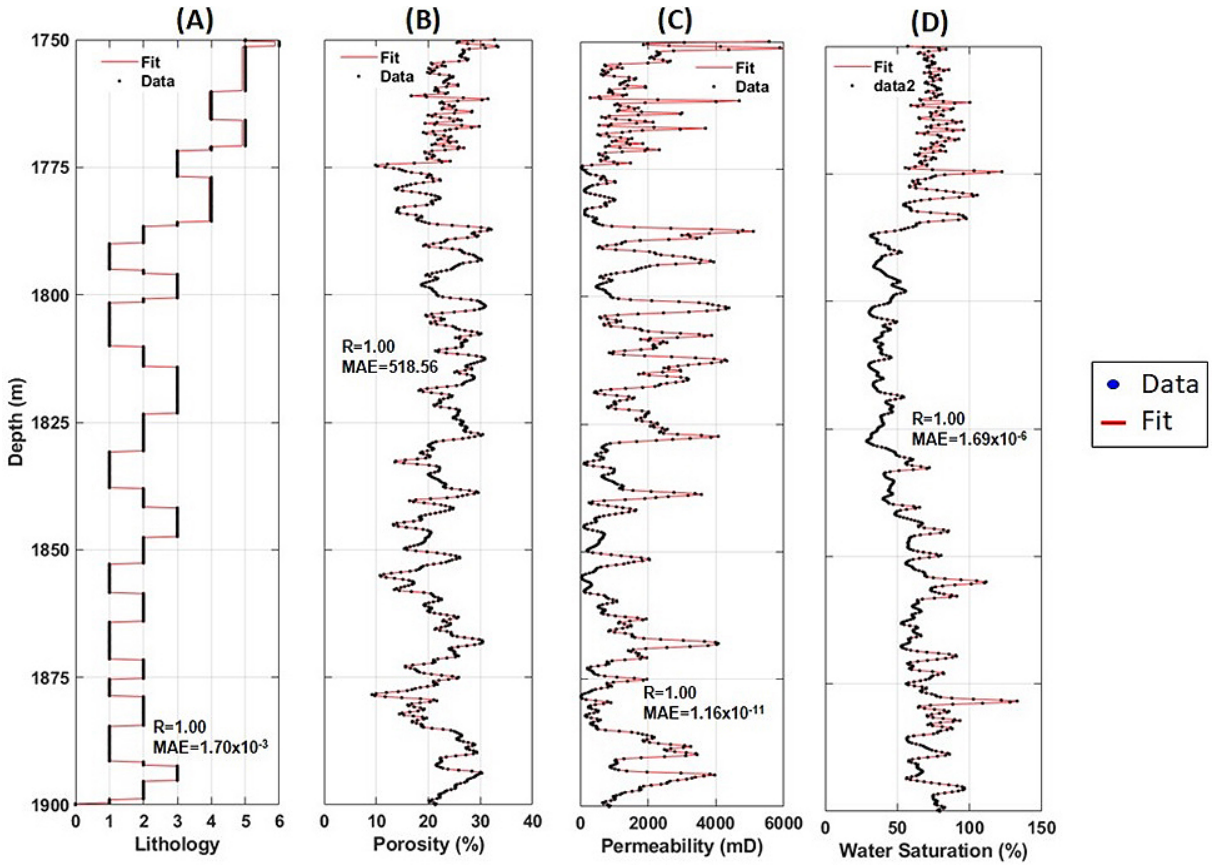

Figure 11. Lithology (a), porosity (b), permeability (c), and water saturation (d) estimates for the blind test well LI03 using the Bayesian Regularization approach.

5. Discussion

The results demonstrate the efficacy of backpropagation neural networks (BPNN) in estimating petrophysical properties of carbonate reservoirs, with Bayesian Regularization (trainBR) outperforming Levenberg-Marquardt (trainLM) and Scaled Conjugate Gradient (trainSCG) in most cases. For lithology estimation, trainBR achieved a near-perfect correlation coefficient ($R = 0.99$) and minimal mean squared error ($MSE = 1.71 \times 10^{-4}$), surpassing the performance reported by Silva et al. (2015), who used ANN for lithology classification but achieved lower accuracy ($R \approx 0.90$). This improvement can be attributed to the robust regularization in trainBR, which mitigates overfitting – a common challenge in lithology prediction (Dell'Aversana, 2019).

Porosity estimation also yielded strong results, with trainBR achieving $R = 0.97$ and $MSE = 0.11$, comparable to the findings of Hamada and Elshafei (2009), who reported $R = 0.95$ for porosity prediction in sandstone reservoirs using conventional logs. However, our study incorporated a broader dataset, including laboratory measurements and geological context, enhancing model reliability. The slightly lower performance of trainLM and trainSCG ($R = 0.87$ and 0.80, respectively) aligns with observations by Mohaghegh et al. (1995) and Carrasquilla and Rocha (2025), who noted that simpler ANN architectures may struggle with heterogeneous carbonate porosity distributions.

Permeability proved the most challenging parameter to estimate, with trainBR yielding $R = 0.97$ but high MSE (7.21×10^5), reflecting the inherent complexity of permeability in carbonates. This aligns with Rezaee et al. (2006), who emphasized the difficulty of permeability prediction due to its dependence on pore structure. While our results are comparable to those of Yeganeh et al. (2012) ($R = 0.92$), our use of advanced BPNN algorithms and integrated datasets provided a more comprehensive approach, particularly in handling extreme permeability variations.

Water saturation estimation was highly accurate, with trainBR achieving $R = 1.00$ and $MSE = 4.74 \times 10^{-9}$, outperforming traditional Archie-based methods and ANN approaches like those of Masoudi et al. (2012), who reported $R \approx 0.90$. The success here likely stems from the synergistic use of resistivity logs and Bayesian regularization, effectively handling nonlinear relationships in the data. This contrasts with simpler models that often overlook log-fluid interactions.

The blind test in well LI03 further validated the methodology, with trainBR achieving perfect correlations ($R = 1.00$) for all parameters. These results surpass those of Bruce et al. (2000), who reported $R \approx 0.85 – 0.95$ for similar blind tests in siliciclastic reservoirs. The consistency underscores the adaptability of BPNN, particularly trainBR, to unseen data – a critical advantage for reservoir characterization where data scarcity is common (Ahmadi et al., 2013).

6. Conclusions

This study presents a backpropagation neural network approach using field log data and laboratory measurements from an Albian carbonate reservoir in the Linguado oilfield, Campos Basin, Southeastern Brazil. The preliminary petrophysical interpretation revealed average porosity and density values of 23% and 2.4 g/cm³, respectively, consistent with a carbonate reservoir.

GR and DT log analysis indicated the reservoir is located between 1760 and 1880 m depth, while a significant increase in resistivity (RT) values from <10 to $>10^4$ Ω·m between 1760 and 1780 m depth confirmed the presence of hydrocarbons.

Artificial neural networks (ANNs) were employed to estimate lithology, porosity, permeability, and water saturation using the Levenberg-Marquardt (trainLM), Scaled Conjugate Gradient (trainSCG), and Bayesian Regularization (trainBR) approaches. While trainLM and trainSCG incorporated training, validation, and testing stages, trainBR utilized only training and testing.

The ANN models demonstrated accurate and efficient predictions for both the reference and blind test wells, validating the reliability of the methodology. Lithology and water saturation estimates showed particularly high accuracy, while porosity predictions were also satisfactory. Permeability estimation proved more challenging, likely due to the greater complexity and variability of this parameter within carbonate reservoirs. Among the ANN approaches, Bayesian Regularization consistently outperformed the other methods, especially for water saturation, highlighting its robustness and potential for broader applications in petrophysical analysis.

Acknowledgements. The authors thank the National Council for Scientific and Technological Development (CNPq) at the Ministry of Science, Technology, and Innovations (MCTI) of Brazil for the research grant, the Petroleum Engineering and Exploration Laboratory (UENF/LENEP) for the computing infrastructure, Geoactive Limited for the academic license of Interactive Petrophysics software, the National Geophysical Science and Technology Institute (INCT-GP), and the Brazilian National Agency of Petroleum, Natural Gas and Biofuels (ANP) by the dataset.

References

Ahmadi, M. A., S. Zendehboudi, A. Lohi, A. Elkamel et al. (2013). Reservoir permeability prediction by neural networks combined with hybrid genetic algorithm and particle swarm optimization, Geophys. Prospect., 61, 3, 582-598, doi:10.1111/j.1365-2478.2012.01080.x.

ANP, National Agency of Petroleum (2019). Natural Gas and Biofuels, Bull. Oil Nat. Gas Prod., External Circulation, 101, Development and Production Superintendence (SDP), January, Rio de Janeiro, 32, in Portuguese.

Archie, G. (1942). The electrical resistivity log as an aid in determining some reservoir characteristics, J. Pet. Technol., 146, 54-62, doi:10.2118/942054-G.

Arthur, C. K., V. A. Temeng and Y. Y. Ziggah (2020). Performance evaluation of training algorithms in backpropagation neural network approach to blast-induced ground vibration prediction, Ghana Min. J., 20, 1, 20-33, doi:10.4314/gm.v20i1.3.

Babani, L., S. Jadhav and B. Chaudhari (2016). Scaled conjugate gradient based adaptive ANN control for SVM-DTC induction motor drive, in Artificial Intelligence Applications and Innovations, 12th IFIP WG 12.5 International Conference and Workshops, AIAI 2016, Thessaloniki, Greece, September 16-18, 2016, Proceedings 12, edited by I. Maglogiannis et al., Springer, Cham, 384-395, doi:10.1007/978-3-319-44944-9_33.

Beale, M. H., M. T. Hagan and H. B. Demuth (2010). Neural Network Toolbox: User's Guide, MathWorks, Natick, MA, 2, 77-81.

Bruce, A., P. M. Wong, Y. Zhang, H. A. Salisch et al. (2000). A state-of-the-art review of neural networks for permeability prediction, APPEA J., 40, 1, 341-354, doi:10.1071/AJ99019.

Bruhn, C. H., J. A. T. Gomes, C. Del Lucchese Jr. and P. R. Johann (2003). Campos Basin: reservoir characterization and management-historical overview and future challenges, in Offshore Technology Conference, OTC-15220, OTC, doi:10.4043/15220-MS.

Cannon, S. (2016). Petrophysics: A Practical Guide, John Wiley & Sons, Hoboken, NJ, 336.

Carrasquilla, A. and R. Lima (2020). Basic and specialized geophysical well logs to characterize an offshore carbonate reservoir in the Campos Basin, southeast Brazil, J. South Am. Earth Sci., 98, 102436, doi:10.1016/j.jsames.2022.104059.

Carrasquilla, A. and H. Rocha (2025). Porosity estimates in an Albian carbonate reservoir in southeastern Brazil using basic well logs, core sample measurements, and fuzzy logic approach. South Am. Earth Sci., 165, 105735, doi:10.1016/j.jsames.2025.105735.

Da Costa, J. L. S., A. A. G. Carrasquilla, A. M. V. Carrasco and H. O. da Rocha (2019). Forward modeling of electric and electromagnetic resistive logs with piston and annular invasion types in pre-salt carbonate reservoirs of the Santos Basin, Brazil, J. Pet. Sci. Eng., 178, 216-226, doi:10.1016/j.petrol.2019.03.038.

Dell'Aversana, P. (2019). Comparison of different Machine Learning algorithms for lithofacies classification from well logs, Boll. Geofis. Teor. Appl., 60, 1, 1-16, doi:10.4430/bgta0256.

Draper, N. R. (1998). Applied regression analysis bibliography update 1994-97, Commun. Stat. Theory Methods, 27, 10, 2581-2623, doi:10.1080/03610929808832244.

Foresee, F. D. and M. T. Hagan (1997). Gauss-Newton approximation to Bayesian learning, in Proc. Int. Conf. Neural Netw., ICNN'97, 3, 1930-1935, IEEE, doi:10.1109/ICNN.1997.614194.

Hamada, G. M. and M. A. Elshafei (2009). Neural network prediction of porosity and permeability of heterogeneous gas sand reservoirs, in SPE Kingdom of Saudi Arabia Annual Technical Symposium and Exhibition, SPE-126042, SPE.

Howard, D. and M. Beale (2000). Neural Network Toolbox for Use with MATLAB: User's Guide, Version 4, MathWorks, Natick, MA, 133-205.

Kaur, H. and D. S. Salaria (2013). Bayesian regularization-based neural network tool for software effort estimation, Glob. J. Comput. Sci. Technol., 13, 2, 44-50.

Luthi, S. M. and I. D. Bryant (1997). Well-log correlation using a back-propagation neural network, Math. Geol., 29, 413-425, doi:10.1007/BF02769643.

Martinez, W. L. and A. R. Martinez (2001). Computational Statistics Handbook with MATLAB, Chapman and Hall/CRC, Boca Raton, FL, 480.

Masoudi, P., B. Tokhmechi, M. A. Jafari, S. M. Zamanzadeh and S. Sherkati (2012). Application of Bayesian in determining productive zones by well log data in oil wells, J. Pet. Sci. Eng., 94, 47-54, doi:10.1016/j.petrol.2012.06.028.

Matlab (2014). User's Manual, MathWorks, www.mathworks.com.

Møller, M. F. (1993). A scaled conjugate gradient algorithm for fast supervised learning, Neural Netw., 6, 4, 525-533, doi:10.1016/S0893-6080(05)80056-5.

Mohaghegh, S., R. Arefi, I. Bilgesu, S. Ameri et al. (1995). Design and development of an artificial neural network for estimation of formation permeability, SPE Comput. Appl., 7, 06, 151-154, doi:10.2118/28237-PA.

Mohebbi, A., R. Kamalpour, K. Keyvanloo and A. Sarrafi (2012). The prediction of permeability from well logging data based on reservoir zoning, using artificial neural networks in one of an Iranian heterogeneous oil reservoir, Pet. Sci. Technol., 30, 19, 1998-2007, doi:10.1080/10916466.2010.518187.

Okubo, J., R. Lykawka, L. V. Warren, J. Favoreto et al. (2015). Depositional, diagenetic, and stratigraphic aspects of carbonates from the Macaé Group (Albian): an example of an oil field in the Campos Basin, Brazil. J. Geol., 45, 2, 243-258, doi:10.1590/2317488920150020005.

Peng, J. X., K. Li and G. W. Irwin (2008). A new Jacobian matrix for optimal learning of single-layer neural networks, IEEE Trans. Neural Netw., 19, 1, 119-129, doi:10.1109/TNN.2007.903150.

Rene, E. R., M. E. López, J. H. Kim and H. S. Park (2013). Back Propagation Neural Network Model for Predicting the Performance of Immobilized Cell Biofilters Handling Gas-Phase Hydrogen Sulphide and Ammonia, Bio. Med. Res. Int., 2013, 1, 463401, doi:10.1155/2013/463401.

Rezaee, M. R., A. Jafari and E. Kazemzadeh (2006). Relationships between permeability, porosity and pore throat size in carbonate rocks using regression analysis and neural networks, J. Geophys. Eng., 3, 4, 370-376, doi:10.1088/1742-2132/3/4/008.

Silva, A. A., I. A. L. Neto, R. M. Misságia, M. A. Ceia et al. (2015). Artificial neural networks to support petrographic classification of carbonate-siliciclastic rocks using well logs and textural information, J. Appl. Geophys., 117, 118-125, doi:10.1016/j.jappgeo.2015.03.027.

Silva, A. A., M. W. Tavares, A. Carrasquilla, R. Misságia et al. (2020). Petrofacies classification using machine learning algorithms, Geophysics, 85, 4, WA101-WA113, doi:10.1190/geo2019-0439.1.

Stone, J. (2015). Bayes' Rules with MATLAB: A Tutorial Introduction to Bayesian Analysis, 1st ed., Sebtel Press, Sheffield, UK, 43.

Tiab, D. and E. Donaldson (2004). Petrophysics: Theory and Practice of Measuring Reservoir Rock and Fluid Transport Properties, 2nd ed., Gulf Professional Publishing, Oxford, 976.

Tweedale, J. W. and L. C. Jain (2014). Advances in Modern Artificial Intelligence, Springer, Cham, 1-18.

Winter, W. R., R. J. Jahnert and A. B. França (2007). Campos Basin, Petrobras Geosci. Bull., 15, 2, 511-529, in Portuguese.

Yang, S. and J. Wei (2017). Fundamentals of Petrophysics, Springer, Berlin, 474.

Yeganeh, M., M. Masihi and S. Fatholahi (2012). The estimation of formation permeability in a carbonate reservoir using an artificial neural network, Pet. Sci. Technol., 30, 10, 1021-1029, doi:10.1080/10916466.2010.512879.

***CORRESPONDING AUTHOR: Herson ROCHA,**

Polytechnic Institute (IPOLI), Federal University of Rio de Janeiro (UFRJ), Rio de Janeiro, Brazil

e-mail: herson.rocha@macae.ufrj.br